ELSEVIER

Journal of Nuclear Materials 270 (1999) 322–333

journal of nuclear materials

Corrosion characteristics and oxide microstructures of Zircaloy-4 in aqueous alkali hydroxide solutions

Y.H. Jeong [a,*], J.H. Baek [a], S.J. Kim [a], H.G. Kim [a], H. Ruhmann [b]

[a] *Nuclear Fuel Cladding Team, Korea Atomic Energy Research Institute, P.O. Box 105, Yusong, Taejon 305-600, South Korea*
[b] *Siemens AG, Power Generation Group (KWU), D-91058 Erlangen, Germany*

Received 6 May 1998; accepted 5 December 1998

Abstract

The corrosion characteristics of Zircaloy-4 have been investigated in various aqueous solutions of LiOH, NaOH, KOH, RbOH and CsOH with equimolar M^+ and OH^- at 350°C. The characterization of the oxides was performed using transmission electron microscope (TEM) and scanning electron microscope (SEM) on the samples which were prepared to have an equal oxide thickness in pre-transition and post-transition regimes. At a low concentration (4.3 mmol) of aqueous alkali hydroxide solutions, the corrosion rates decrease gradually as the ionic radius of cation increases. At a high concentration (32.5 mmol), the corrosion rate increases significantly in LiOH solution and slightly in NaOH solution, but in the other hydroxide solutions such as KOH, RbOH and CsOH, the corrosion rate is not accelerated. Even if the specimens have an equal oxide thickness in LiOH, NaOH and KOH solutions, the oxide microstructure formed in the LiOH solution is quite different from those formed in the NaOH or the KOH solutions. In the LiOH solution, the oxides grown in the pre-transition regime as well as in the post-transition regime have an equiaxed structure including many pores and open grain boundaries. The oxides grown in the NaOH solution have a protective columnar structure in the pre-transition regime but an equiaxed structure in the post-transition regime. On the other hand, in the KOH solution, the columnar structure is maintained from its pre-transition regime to the post-transition regime. On the basis of the above results, it can be suggested that the cation incorporation into zirconium oxide would control the oxide microstructure, the oxide growth mechanism at the metal–oxide interface and the corrosion rate in alkali hydroxide solutions. © 1999 Elsevier Science B.V. All rights reserved.

PACS: 28.41.T; 81.65.M; 42.81.B

1. Introduction

The corrosion on the fuel cladding still remains a major concern even if numerous studies have been performed for several decades. In particular, the corrosion of fuel cladding for high burn-up fuel plays an important factor in the lifetime of fuel cladding. Lithium hydroxide is added to the primary coolant for pH control and thereby reduces the activation out of core components. It is well known that the high concentration of LiOH accelerates the corrosion of zirconium alloys not only in in-reactor where local boiling occurs at the surface of the fuel rod, but also in the autoclave where isothermal condition is maintained.

Numerous studies on the effect of LiOH on the corrosion of zirconium have been performed. Concerning the critical concentration of LiOH in an aqueous solution to accelerate the corrosion of Zircaloy, Garzarolli et al. [1] and McDonald et al. [2] reported that the corrosion enhancement occurred in the concentration with more than 30 ppm lithium in the solution and 100 ppm lithium in the oxide, respectively. Since the lithium is added as a form of lithium hydroxide, one species or two species among Li^+, OH^- (or pH) and LiOH can influence the corrosion acceleration of zirconium alloys. Hillner and Chirigos [3] reported that the corrosion in 1

* Corresponding author. Tel.: +82-42 868 2322; fax: +82-42 868 8346; e-mail: ywjeong@nanum.kaeri.re.kr.

0022-3115/99/$ – see front matter © 1999 Elsevier Science B.V. All rights reserved.
PII: S0022-3115(99)00008-2

mol LiOH solution occurred 25 times faster than that in 1 mol KOH solution and so Li^+ would be a main species to control the corrosion acceleration. On the other hand, they also observed that the corrosion acceleration occurred only in LiOH solution and did not occur in $LiNO_3$ solution. Therefore, what accelerated the corrosion might be Li^+ even though it did not affect the corrosion independently.

Perkins and Busch [4] showed that the pH of the corrosion solution decreased from 12.3 to 10.3 by the conversion of LiOH into Li-carbonate when LiOH solution was exposed to the air environment and then the corrosion rate came down rapidly. Moreover, it was reported that the addition of H_3BO_3 to LiOH solution decreased the corrosion rate of the Zircaloy-4 as well as the pH of the LiOH solution [5,6]. Ramasubramanian et al. [7,8] and Cox et al. [9,10] reported that the undissociated LiOH itself in the solution accelerated the corrosion, together with the formation of the porous oxide. On the other hand, it was observed in the previous work [11] that the corrosion rate decreased in order of LiOH, NaOH, KOH, RbOH and CsOH solutions in the autoclave conditions at 350°C for 150 days.

Several mechanistic models have been suggested to explain the corrosion acceleration in LiOH solution. With the growth of an oxide layer, the substitution of Li^+ for Zr^{4+} site would cause the increase of oxygen vacancy concentration that could accelerate the corrosion in LiOH solution [3]. It was also reported that the corrosion of the Zircaloy-4 was closely related to the ionic radius of group-1 alkali metal [11]. The modified crystal growth mechanism was suggested by Garzarolli et al. [12] that an alkalizer like LiOH accelerated the corrosion because it modified the mechanism of the crystal growth. In other words, the LiOH caused the oxide structure to be equiaxed, not to be columnar. The undissociated LiOH could have an influence on the formation of porous oxide layer resulting in the accelerated corrosion [7,8]. Also, Cox et al. [10] said that the porous oxide would be formed by the dissolution and the reprecipitation of the oxide in LiOH solution and the boric acid could have a plugging effect on the pores in the oxide layer. However, unfortunately, it has not been apparently known regardless of the above numerous experimental results, which if any of Li^+, OH^- and LiOH species accelerate the corrosion of the zirconium-based alloy in LiOH solution.

On the other hand, the microstructural study on the oxide will be needed to understand the corrosion mechanism on the nuclear fuel cladding. Recently, it was reported by Garzarolli et al. [12] from the TEM studies on the oxide that due to the mineralizing effect of hydrogen, the uniform oxide that consisted of the columnar structure showed good corrosion resistance, whereas the nodular oxide that consisted of the equiaxed structure showed accelerated corrosion. Beie et al. [13] also reported that the uniform oxide consisted of the columnar structure of monoclinic ZrO_2 with a small volume fraction of tetragonal ZrO_2 and the nodular oxide consisted of the equiaxed grain with the numerous open pores.

According to the TEM results on the oxide formed in LiOH solution, as reported by Pêcheur et al. [14], the oxide formed before the acceleration consisted of the columnar grains and the Li element did not reach the metal–oxide interface, whereas after the acceleration the oxide near the metal–oxide interface consisted mainly of the equiaxed grain and the outer part maintained the columnar grain which formed at the early stage, where Li^+ could reach to the interface. Thus, they suggested that the degree of the accelerated corrosion in the LiOH solution was dependent on how the dense inner layer protected the ingress of the Li^+ into the metal. Anada and Takeda [15] reported that the change of the columnar ZrO_2 into the equiaxed ZrO_2 mainly occurred near the lateral crack or the incorporated precipitate and the tetragonal ZrO_2 and the sub-ZrO_2 played an important role in controlling the corrosion.

From the numerous TEM studies on the oxide, it is summarized that the oxide characteristics are dependent on the oxide thickness, the oxide type and the corrosion conditions. However, the microstructures formed in the different alkali hydroxide solutions were not evaluated, in particular, on the oxides having an equal oxide thickness. That is helpful to evaluate the mechanistic aspects of the accelerated corrosion in alkalized environments.

In this study, from the long-term corrosion test in various group-1 alkali hydroxide solutions the corrosion behavior with the ionic radius of alkali metal is clearly evaluated. And the oxide growth mechanism with the corrosion time is also investigated by observing the oxide microstructure and the oxide morphology on the Zircaloy-4 corroded in equimolar LiOH, NaOH and KOH solutions.

2. Experimental procedure

Two kinds of specimens, Zircaloy-4 cladding and Zircaloy-4 sheet, were used for the corrosion test to investigate the effect of LiOH and the effect of alkali hydroxide on the corrosion, respectively. The final stress relieving temperature of the Zircaloy-4 cladding tube containing 1.44 wt% Sn, 0.21 wt% Fe and 0.11 wt% Cr was 490°C. The chemical composition of Zircaloy-4 sheet with recrystallized condition was 1.51 wt% Sn, 0.22 wt% Fe and 0.11 wt% Cr. The specimens were chemically polished using a pickling solution before the corrosion tests. The corrosion tests to investigate the corrosion behaviors in LiOH solutions were conducted in aqueous LiOH solutions in the static autoclave at

350°C under a pressure of 17 MPa. Li was added as LiOH with the concentrations of 2.2 ppm (0.32 mmol), 30 ppm (4.3 mmol), 220 ppm (32.5 mmol) and 2200 ppm (325 mmol), where 2.2 ppm represents the normal concentration in the primary PWR coolant and 30 ppm is known to the concentration for onset of Li-enhanced corrosion under isothermal condition [1].

Table 1 shows the summary on the concentration of alkali hydroxide solutions used for corrosion test to evaluate the corrosion behaviors in various alkali hydroxides. The corrosion tests were performed in LiOH, NaOH, KOH, RbOH and CsOH solutions of 4.3 and 32.5 mmol with equimolar M^+ and OH^-, where 4.3 mmol corresponds to 30 ppm Li, 99 ppm Na, 169 ppm K, 360 ppm Rb and 574 ppm Cs and 32.5 mmol corresponds to 220 ppm Li, 724 ppm Na, 1231 ppm K, 2692 ppm Rb and 4186 ppm Cs. The corrosion resistance of the specimens were characterized by measuring their weight gains with the exposure time.

To investigate the microstructures of the oxides formed in LiOH, NaOH and KOH solutions, two kinds of the corroded specimens were prepared to have the weight gains of about 25 mg/dm^2 (approximately corresponding to 1.7 μm oxide thickness) and about 60 mg/dm^2 (approximately corresponding to 4.0 μm oxide thickness) which represent the weight gains before and after the transition point, respectively. The microstructures of the oxides were observed and analyzed for the specimens having equal weight gains using a TEM. TEM specimens for the observation of oxide microstructures were prepared in a sequence of cutting, grinding and polishing. Finally thin foil was prepared by Ar ion milling.

The morphologies of oxide at the oxide–metal interface after the corrosion tests were observed using SEM after dissolving completely the metal part with a mixing solution of 10% HF, 45% HNO_3 and 45% H_2O. The amounts of hydrogen pickup in the corroded specimens were also quantitatively analyzed by using the hot extraction method and hydrogen analyzer (LECO). Before hydrogen analysis of corroded specimens, the oxide films were removed by sand blasting.

3. Results

3.1. Corrosion behaviors of the Zircaloy-4 cladding in aqueous LiOH solutions

Fig. 1 shows the corrosion behaviors of the Zircaloy-4 cladding in aqueous LiOH solution with various Li concentrations at 350°C for 550 days. In pure water, the Zircaloy-4 shows a typical cyclic corrosion behavior with the continuous increase of the corrosion rate having the first transition at about 180 days, the second transition at about 330 days and so on. It was reported that the cyclic corrosion behavior for the Zircaloy-4 cladding originated from the continuous formation of a new oxide layer between the non-protective oxide layer and the metal, where the protective oxide layer which was formed at an early stage transformed into the non-protective oxide with the increase of the oxide thickness [12,16–19].

In an aqueous 2.2 ppm LiOH solution, the normal concentration in the PWR primary coolant, the Zircaloy-4 cladding shows almost the same corrosion behavior as that in the pure water condition. In an aqueous 30 ppm LiOH solution, it also shows the similar behavior to that in the pure water over all range, but the first transition (at about 100 days) occurs earlier compared to its behavior in the pure water condition. The difference in the weight gains obtained from the pure water and the aqueous 30 ppm LiOH solution increases continuously with the increase in the exposure time.

It is thought from these results that the critical concentration of Li to accelerate the corrosion would be between 2.2 and 30 ppm since the corrosion of Zircaloy-4 is accelerated in aqueous 30 ppm LiOH solution. In the solution containing the Li-concentration of more than 220 ppm, the corrosion rate is significantly accel-

Table 1
Summary of the concentration of alkali hydroxide solutions used for corrosion test

Alkali hydroxide	Concentration of M^+		Concentration of OH^-		pH at 25°C	
	mmol	ppm	mmol	ppm	Calculated	Measured
LiOH	4.3	30	4.3	73	11.6	11.4
NaOH	4.3	99	4.3	73	11.6	11.4
KOH	4.3	169	4.3	73	11.6	11.4
RbOH	4.3	369	4.3	73	11.6	11.5
CsOH	4.3	574	4.3	73	11.6	11.5
LiOH	32	220	32	535	12.5	12.2
NaOH	32	724	32	535	12.5	12.2
KOH	32	1231	32	535	12.5	12.3
RbOH	32	2692	32	535	12.5	12.4
CsOH	32	4186	32	535	12.5	12.4

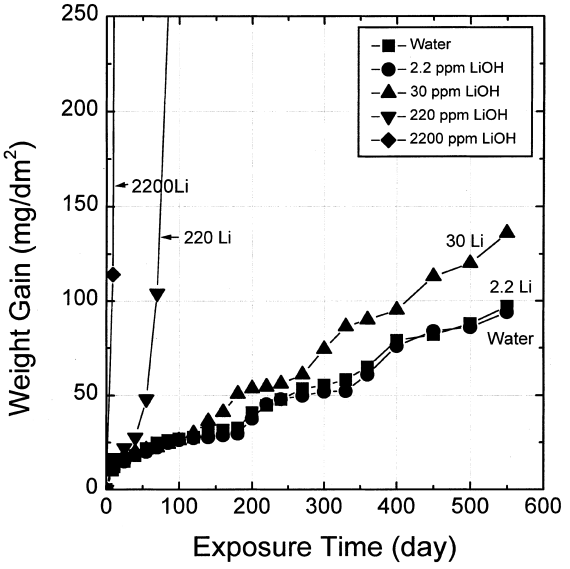

Fig. 1. Corrosion behavior of Zircaloy-4 cladding in aqueous LiOH solutions at 350°C.

erated, but the cyclic corrosion behaviors of corrosion rate is not shown.

3.2. Corrosion behaviors of the Zircaloy-4 sheet in LiOH, NaOH, KOH, RbOH and CsOH solutions

It was reported by Jeong et al. [11] from the results obtained in various alkali hydroxide solutions that the accelerated corrosion of zirconium alloys in the aqueous LiOH solution was mainly due to the existence of Li^+. In that paper the specimens showed the corrosion behaviors at the post-transition regime only in the LiOH solution but those at the pre-transition in other alkali solutions due to the short exposure time. In this paper, therefore, the extended corrosion tests were carried out to confirm the long-term behaviors of Zircaloy-4 for 300 days using the recrystallized Zircaloy-4 sheets in equimolar aqueous LiOH, NaOH, KOH, RbOH and CsOH solutions.

Fig. 2 shows the corrosion behaviors of the Zircaloy-4 sheet corroded in various aqueous alkaili hydroxide solutions with the concentration of 4.3 and 32.5 mmol

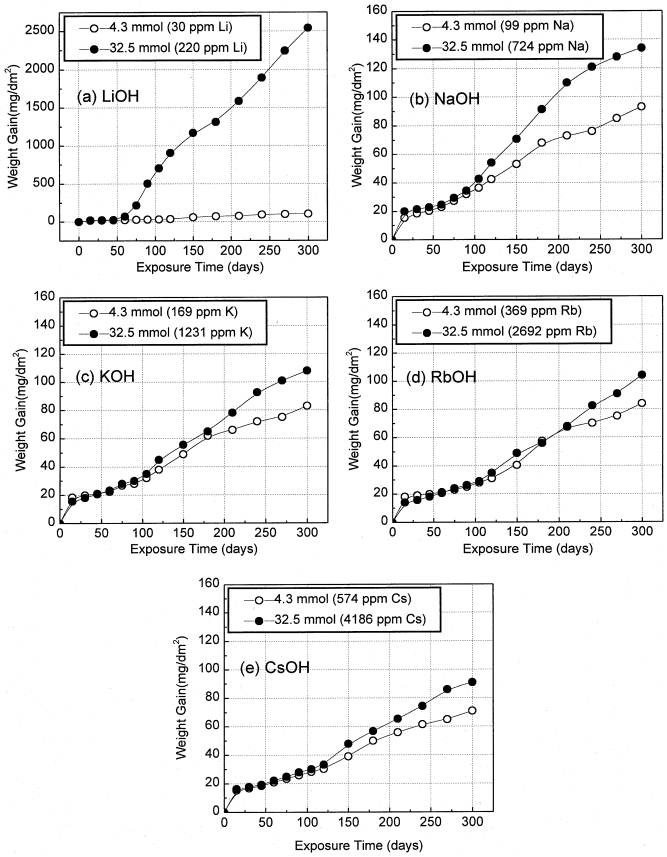

Fig. 2. Corrosion behavior of Zircaloy-4 sheet in various alkali hydroxide solutions at 350°C.

for 300 days. As shown in Fig. 2(a), in the aqueous 4.3 mmol LiOH solution, the weight gains of the Zircaloy-4 sheet increase slightly with the increase of the exposure time. However, in the aqueous 32.5 mmol LiOH solution, the weight gain of the Zircaloy-4 sheet starts to increase rapidly at 45 days. As shown in Fig. 2(b), in the aqueous NaOH solution, the corrosion rate increases rapidly after 60 days in both concentrations. That means that the transition of the corrosion rate occurs about 60 days in these test conditions. However, as compared to the corrosion in high concentration of LiOH solution, the corrosion in high concentration of NaOH is not significantly accelerated even after 300 days, showing the low weight gain of 130 mg/dm^2 at that exposure time. The corrosion behaviors in aqueous KOH, RbOH and CsOH solutions as shown in Fig. 2(c)–(e), respectively, are very similar to that in aqueous NaOH solution. All the weight gains in aqueous KOH, RbOH and CsOH solutions after 300 days test indicate the corrosion behaviors in post-transition regime. However, the transition time that occurred the rapid increase of the corrosion rate is increased in order of KOH, RbOH and CsOH solutions.

Fig. 3 shows the comparison of corrosion behaviors in the various alkali hydroxide solutions with the concentrations of 4.3 and 32.5 mmol. In the 4.3 mmol concentration, the weight gains increase gradually with increasing the exposure time. At 300 days the highest weight gain is shown in the LiOH solution and subsequently the weight gains decrease in order of NaOH, KOH, RbOH and CsOH solutions. In the 32.5 mmol concentration, the tendency of corrosion behaviors are also the same as in the case of 4.3 mmol except for the corrosion in aqueous LiOH solution showing the severe acceleration.

The weight gains with the ionic radius of the alkali metal are shown in Fig. 4. The values of the adapted ionic radii are determined for the nearest coordination number (Li, Na = 6, K, Rb and Cs = 8) when it is assumed that Zr^{4+} cation is coordinated with eight oxygen anions in cubic ZrO_2 structure [20]. In 4.3 mmol concentration, the weight gains do not change in the pre-transition regime up to 60 days as the ionic radius of the alkali metal increases. And at the exposure times more than 150 days, the weight gains decrease gradually with increasing the ionic radius of the alkali metal. In 32.5 mmol concentration, the corrosion behaviors with the ionic radius are similar to that in the case of 4.3 mmol except that the specimen corroded only in the aqueous LiOH solution shows severely accelerated corrosion behavior.

Fig. 5 shows the variation of hydrogen pickup fraction with the ionic radius. As the ionic radius of the alkali metal increases, the hydrogen pickup fraction decreases regardless of the concentration of the alkali hydroxide. The hydrogen pickup fractions in the solution having the high concentration of LiOH and NaOH increased compared to those in the low concentration. However, the hydrogen pickup fractions in the cases of aqueous KOH, RbOH and CsOH solutions are almost the same showing about 15% in both transition regimes. It means that the amounts of the hydrogen pickup and the hydrogen pickup fractions become high when the alkali metal in an aqueous alkali hydroxide has a similar size to that of Zr^{4+}. Garzarolli et al. [12] reported that the allotropic transformation of the oxide could be enhanced due to the mineralizing effect by the absorbed hydrogen during the corrosion, which results in accelerating the corrosion.

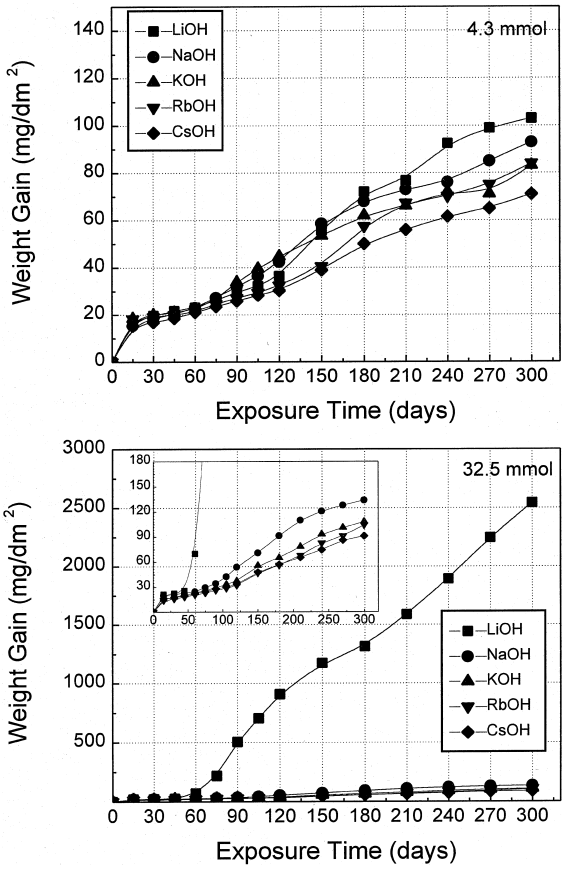

Fig. 3. Comparison of corrosion in various alkali hydroxide solution with equimolar M^+ and OH^- at 350°C.

3.3. TEM observation of the oxide formed in LiOH, NaOH and KOH solutions

Fig. 6 shows the TEM micrographs of oxide formed in LiOH solution. The oxide at the metal–oxide interface in the pre-transition regime as well as the post-transition regime is composed of equiaxed structure. This structure is also observed at the middle of oxide grown in both

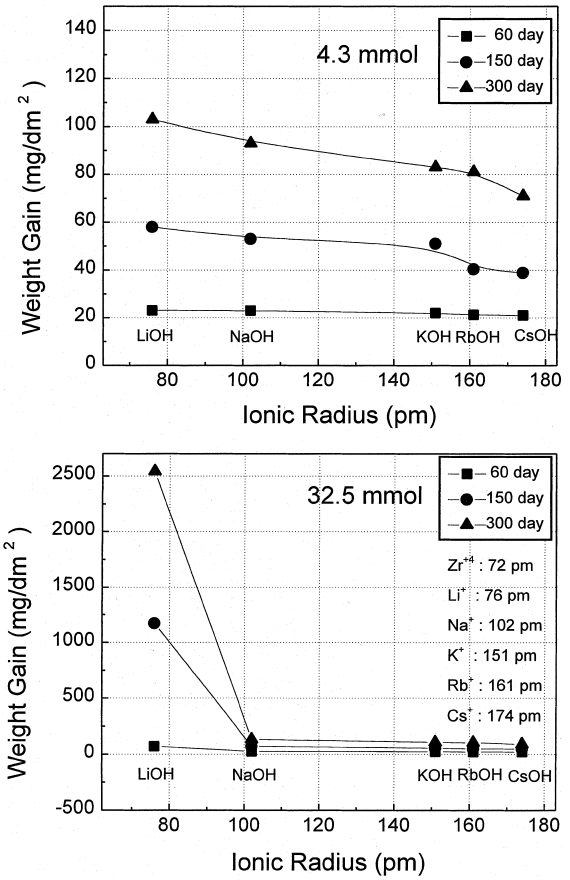

Fig. 4. Weight gain of Zircaloy-4 vs. ionic radius of alkali hydroxide cation.

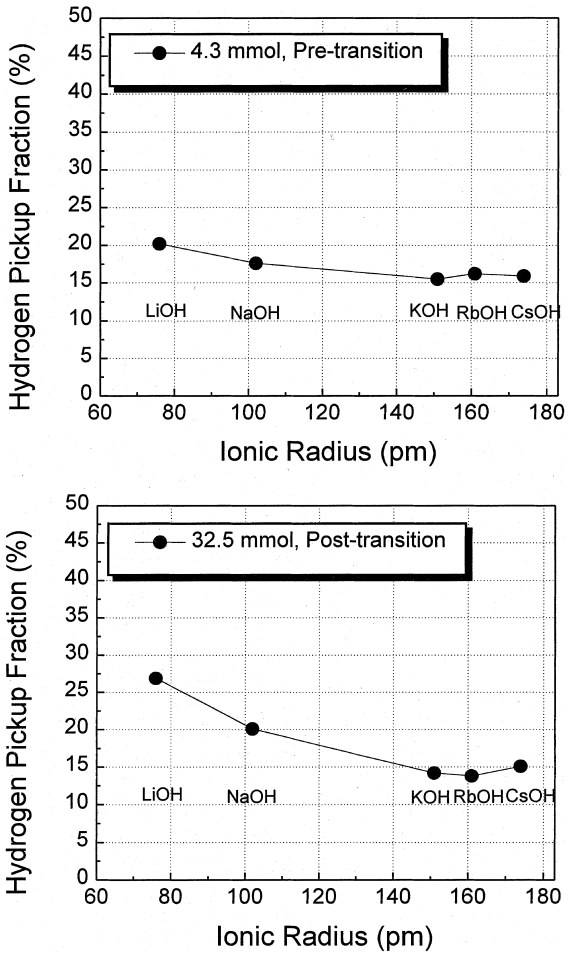

Fig. 5. Hydrogen pickup fraction of Zircaloy-4 in equimolar aqueous alkali hydroxide solutions.

transition regimes. Other investigators [14,15] reported that oxide structures were transformed from the columnar grains in pre-transition regime to the equiaxed grains in post-transition regime. However, in this study the columnar grain is not observed even in pre-transition regime, which means that the columnar grain was not formed or not maintained for such exposure time due to the high corrosion rate in LiOH solution even if it is formed.

The grain sizes of oxides are measured as 15–20 nm in pre-transition regime (Fig. 6(a) and (b)) and 20–25 nm in post-transition regime (Fig. 6(c) and (d)). Many white grain boundaries are observed in the oxides formed in pre-transition regime as well as in post-transition regime. It was reported by Beie et al. [13] and Pêcheur et al. [14] that the white grain boundaries would be open grain boundaries or pores which indicates the weak intergranular cohesion. This observation of the white grain boundaries in the oxide can be supported by the hypothesis proposed by Cox and Wu [9] that LiOH causes a preferential dissolution of zirconia at the grain boundaries.

Fig. 7 shows the TEM micrographs on the oxide formed in NaOH solution. In pre-transition regime the columnar grains with the length of 150–200 nm and the width of 15–20 nm are observed. Even if the corroded samples have an equal oxide thickness in LiOH and NaOH, the columnar grains are observed only in the oxide formed in NaOH solution. The preservation of the columnar grains in NaOH solution would be related to the low corrosion rate in NaOH solution as compared with that in LiOH solution. Nevertheless, in post-transition regime the columnar grains are transformed into the small equiaxed grains with the grain size of 15–20 nm including the many open grain boundaries or pores.

The TEM microstructures of the oxide formed in KOH solution is shown in Fig. 8. The oxide formed in pre-transition regime is mostly composed of the columnar grains but partly of the amorphous oxide at metal–oxide interface, which is not observed in LiOH

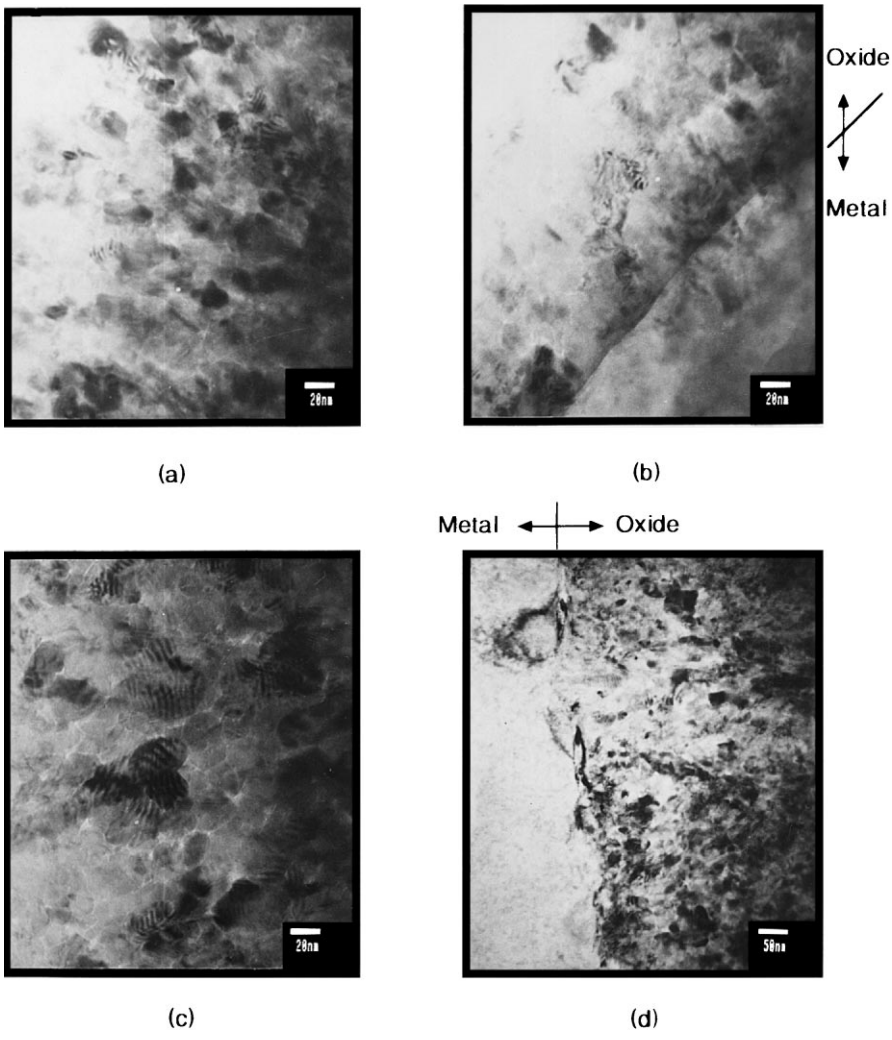

Fig. 6. Cross-sectional TEM micrographs of Zircaloy oxide grown in LiOH solution: (a) at the middle of oxide grown in pre-transition; (b) at metal–oxide interface of oxide grown in pre-transition; (c) at the middle of oxide grown in post-transition; (d) at metal–oxide interface of oxide grown in post-transition.

and NaOH solutions. The amorphous oxide, as illustrated by the electron diffraction pattern in Fig. 8(a), is observed not at the whole area but at the local area of the metal–oxide interface. This amorphous oxide has disappeared in post-transition regime and transformed into the columnar grains, where the porous grain boundaries are not observed, as shown in Fig. 8(b). This means that the oxide formed in KOH solution is more protective and stable than those formed in LiOH and NaOH solutions. The reason for formation of amorphous oxide only in KOH solution is unclear. It could be thought that the amorphous oxide would be related to the oxide stability. Therefore, even though oxide characteristics on the corroded specimens in RbOH and CsOH were not investigated in this study, the possibility to form the amorphous oxide in RbOH and CsOH is not excluded.

3.4. SEM observation of the oxide at metal–oxide interface

Fig. 9 shows the SEM micrographs at the metal–oxide interface of the Zircaloy-4 sheet corroded in LiOH, NaOH and KOH solutions. The SEM morphologies at the metal–oxide interface of the sample corroded in the pre-transition regime of LiOH solution exhibit a uniform thin oxide layer in the greater part of oxide with a large number of the protruded round oxide. However, it is observed that the oxide morphologies at the metal–oxide interface are different from grain to

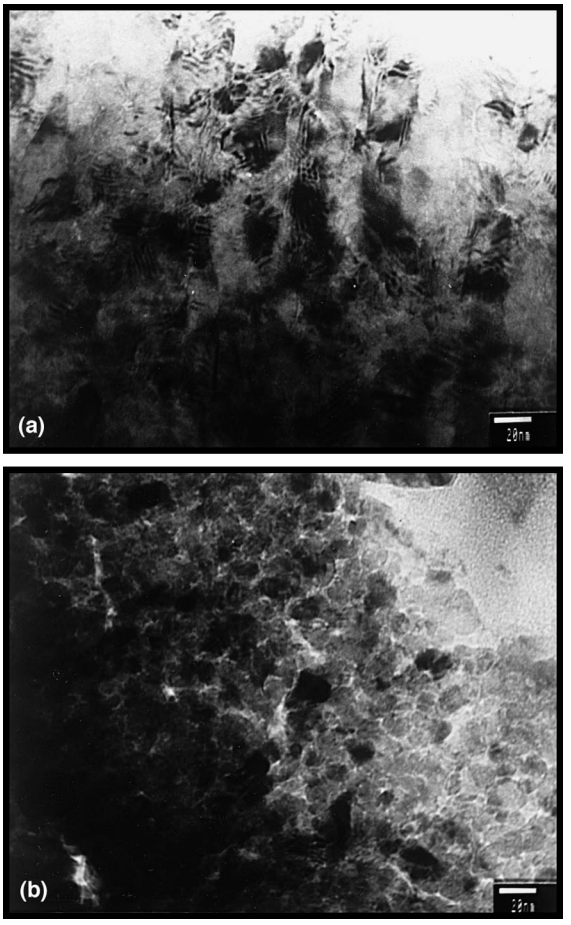

Fig. 7. Cross-sectional TEM micrographs of Zircaloy oxide grown in NaOH solution: (a) pre-transition (25 mg/dm^2); (b) post-transition (60 mg/dm^2).

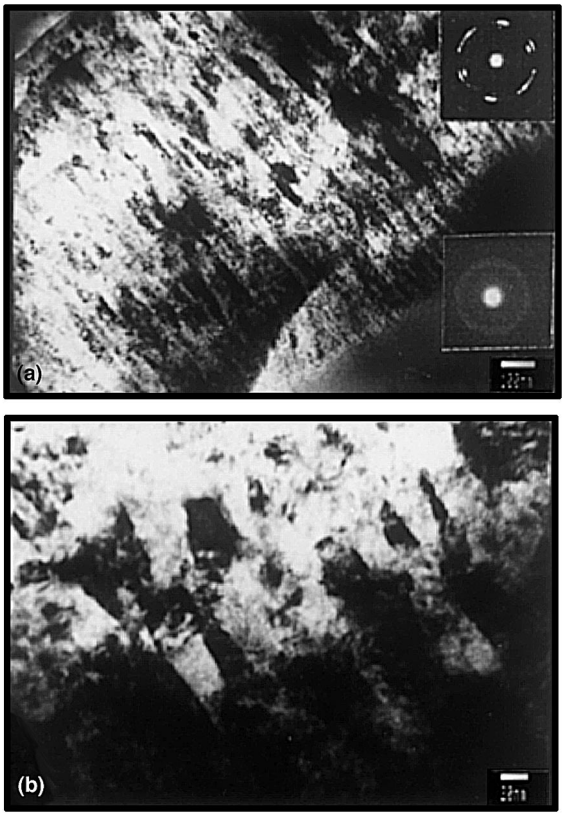

Fig. 8. Cross-sectional TEM micrographs of Zircaloy oxide grown in KOH solution: (a) pre-transition (25 mg/dm^2); (b) post-transition (60 mg/dm^2).

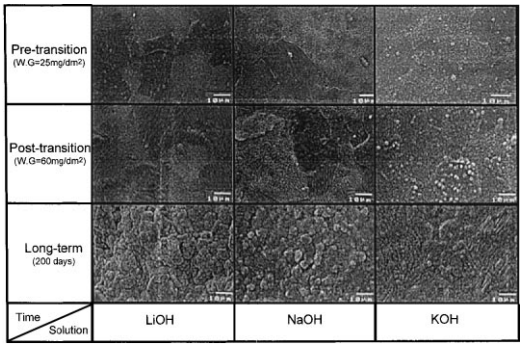

Fig. 9. SEM micrographs at metal–oxide interface of Zircaloy-4 with equal oxide thickness grown in LiOH, NaOH and KOH solution.

grain of the zirconium matrix. It is also observed that the corrosion rate at the grain boundary of zirconium matrix is much faster than that at the interior of the zirconium matrix grain. The oxide morphologies grown in the post-transition regime of LiOH solution represent the shape of ice columns having the different orientation of the oxide growth and the different growth rate of the oxide with varying the grain orientation of metal. In the long-term corrosion test for 200 days in LiOH solution, the ice columnar oxides are transformed into the cauliflower morphologies containing the numerous open pores and cracks between the lump-type oxides.

In NaOH solution, the oxide formed in pre-transition regime shows a dense oxide layer without a protruded round oxide but with a few large lumps, which is identified as a corroded second phase particle by SEM/EDX analysis. The oxides formed in post-transition regime of NaOH solution show the remarkable difference in the oxide morphology with varying the grain orientation of zirconium metal. The width of ice columnar oxides in NaOH solution is much narrower compared to those in LiOH solution. After a long-term corrosion test for 200 days in an NaOH solution, the ice columnar oxides are mainly transformed into the lump-type oxides but still

remained with small fraction. In particular, the cauliflower morphologies of oxides are not observed even after a long-term corrosion test in NaOH solution.

In a KOH solution, the process of oxide development is quite different from those in LiOH and NaOH solution. The numerous small round-type oxides, instead of ice columnar oxides, are formed from the pre-transition regime. This trend continues to the oxide formed in post-transition regime showing the wide dispersion of the round-type oxide. After a long-term corrosion test in KOH solution, the round-type oxide is replaced by the mixed oxides of a columnar-type in a major portion and round-type in a minor portion. In order to confirm that the oxide morphology formed in a KOH solution is quite different from those formed in LiOH and NaOH solutions, a systematic investigation on the development of oxide morphology at the metal–oxide interface was carried.

Fig. 10 shows the variation of oxide morphologies in a KOH solution with increasing weight gain from the earlier stage of oxidation (15 mg/dm^2) to the later stage (100 mg/dm^2). It is confirmed that the numerous small round-type oxides are formed from the earlier stage (15 mg/dm^2) of corrosion and maintained with increasing weight gain up to 45 mg/dm^2. The oxide in the sample having the weight gain of 45 mg/dm^2 shows the two distinguished morphologies, that is, the one fully covered with round-type oxides and the other with a few round-type oxides. As the weight gain increases up to 100 mg/dm^2, these round-type oxides transform into the mixed morphologies of an ice columnar oxide and a round-type oxide. However, the large lump-type oxide showed in LiOH and NaOH solutions are not observed even at the metal–oxide interface with a weight gain of 100 mg/dm^2. Therefore, it can be thought that the growth mechanism of the oxide in a KOH solution be different from those in LiOH and NaOH solutions.

Fig. 11 shows the different oxide growth morphologies depending on the crystal orientation of zirconium metal. Three different oxide morphologies are observed at the metal–oxide interface of the corroded sample having the weight gain of 60 mg/dm^2 in LiOH solution. As shown in Fig. 11(a), A-type oxide shows the very fine and granular morphology and B-type oxide looks like a needle-leaf tree with the orientation of oxide growth. On the other hand, C-type oxide shown in Fig. 11(d) consists of the lump-type oxides containing the numerous cracks and pores at the boundary of lump-type oxide. Therefore, it is considered that the growth rate and the morphology of oxide greatly depend on the crystal orientation of the zirconium matrix. This trend seems to have resulted from the anisotropy of oxygen diffusion in zirconium lattice. Pemsler [21] reported that the corrosion rate is lowest, when the *c*-axis of the hexagonal crystal of zirconium is parallel to the plane of the sample and increases to a maximum when the angle between the *c*-axis and the plane of the sample is about 20°. Bibb and Fascia [22] have determined that if the

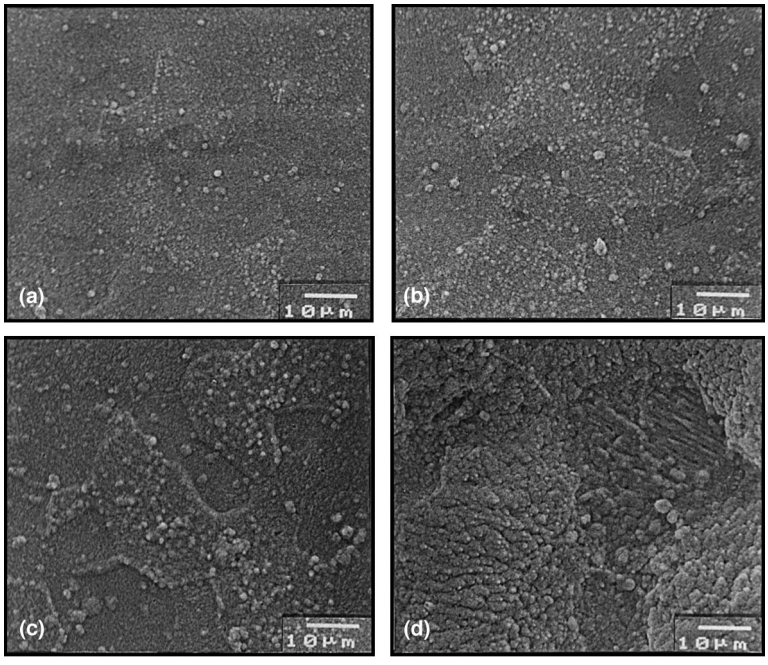

Fig. 10. Developnent of oxide morphology at metal–oxide interface in KOH solution with increasing weight gain: (a) 15 mg/dm^2; (b) 25 mg/dm^2; (c) 45 mg/dm^2; (d) 100 mg/dm^2.

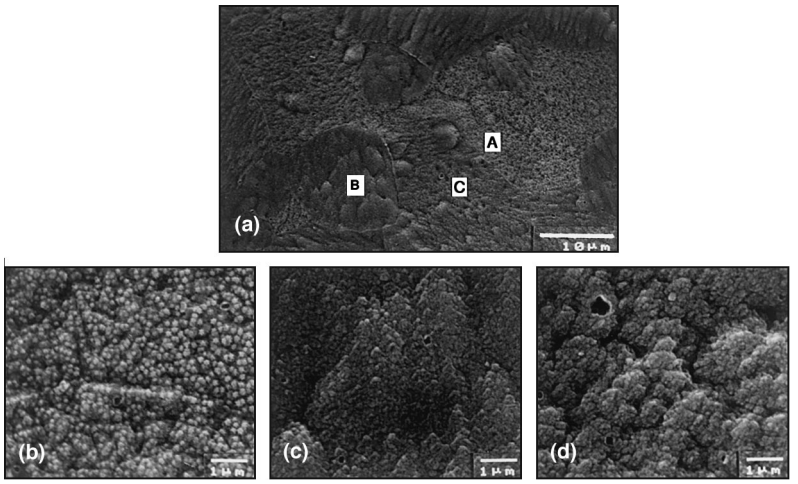

Fig. 11. SEM micrographs showing three different oxide growth morphology at metal–oxide interface of Zircaloy oxide grown in LiOH solution: (a) three different oxide morphology; (b) A-type oxide in (a); (c) B-type oxide in (a); (d) C-type oxide in (a).

sample surface is parallel to the (2 1 $\bar{3}$ 0), the corrosion rate is lowest and if the sample surface is parallel to the (1 0 $\bar{1}$ 2), the corrosion rate is highest. Therefore, although the crystal orientations in each grain of zirconium metal were not measured in this study, it can be thought that A-type oxides with the dense granular morphology would be formed at (0 0 0 1) and B-type oxides showing the high corrosion rate at similar plane to (1 0 $\bar{1}$ 2).

4. Discussion

It was observed that the corrosion rate increased in the Li-concentration more than 30 ppm as shown in Fig. 1. The time to transition of corrosion rate was almost same in pure water and 2.2 ppm Li solution. On the other hand, the transition in 30 ppm Li solution occurred earlier than that in 2.2 ppm Li solution. This means that the transition of corrosion rate would depend on the stability of the barrier oxide layer. Li^+ ion would affect the stability of oxide due to the increase of anion vacancy in barrier layer in 30 ppm Li solution. But the rapid transition of corrosion rate in Li-concentrations more than 220 ppm would be caused by the early transformation of oxide morphology.

From the corrosion results obtained in the equimolar alkali hydroxide solutions, it was observed that the significant acceleration of the corrosion rate of Zircaloy-4 was shown in only aqueous LiOH solution. Therefore, the effect of OH^- ion in the aqueous solution on the corrosion could be excluded by the equimolar M^+ and OH^- condition used in this study. It can be thought that it is easy to substitute Li^+ for Zr^{4+} in the oxide layer due to the similar ionic radii ($Li^+ = 76$ pm and $Zr^{4+} = 72$ pm) whereas it is very difficult for Na^+, K^+, Cs^+ and Rb^+ due to the big difference of ionic radii between cation and Zr^{4+}. Therefore, it could be suggested that the corrosion of the Zircaloy-4 in alkali hydroxide solutions be accelerated by the existence of metallic ion, not by the OH^- ion (or pH). Also, it can be said that the corrosion in aqueous LiOH solution is accelerated owing to the easy substitution of Li^+ for Zr^{4+} in the oxide layer, indicating the formation of many anion vacancies, by the similar size of their ionic radii.

Concerning the oxygen diffusion in the oxide, Cox and Pemsler [23] suggested that the oxygen ion moves into the metal by non-lattice diffusion via the routes, such as grain boundary and pores in the oxide because the lattice diffusion coefficient of oxygen ion is 10^{-4} times as low as the diffusion coefficient measured in the corrosion process at the ranges of 400–500°C. It is thought that the diffusion coefficient and the diffusion routes of oxygen could be dependent on the oxide characteristics. Many investigators [12–14] recently reported that the oxides consisted of the non-protective oxide layer on the outside and the barrier oxide layer near the metal–oxide interface.

Thus, it can be considered that the main governing factor on the corrosion is how fast the oxygen diffusion in the barrier layer occurs, not the oxygen diffusion via the grain boundary or pores in porous outer oxide layer and in the barrier oxide layer the increase of oxygen vacancies resulted from the substitutions of Li^+ for Zr^{4+} could significantly contribute to the acceleration of corrosion as the exposure time increases. It can be said that the accelerated corrosion of the Zircaloy-4 alloys is promoted by the substitution of metallic ion for Zr^{4+} in the oxide layer together with the hydrogen pickup into the metal.

The development of the oxide morphologies with increasing the weight gain in LiOH, NaOH and KOH solutions is schematically summarized in Fig. 12. In a LiOH solution the difference in the growth rate of oxide between the grains of zirconium matrix is observed even in the earlier stage. This trend becomes more remarkable with increasing the weight gain. Owing to the high corrosion rate in LiOH solution, the thick oxide layer showing the fast corrosion can grow much more rapidly as compared to the thin oxide layer showing the slow corrosion rate. This difference in corrosion rate among the zirconium grains results in the non-uniform distribution of the stress at the metal–oxide interface between the slowly corroded area and the rapidly corroded area. The non-uniform distribution of the stress at metal–oxide interface also causes the local acceleration of corrosion and then, ultimately, the cauliflower morphologies having the diameter of $d1$ size (about 6 μm) in the long-term corrosion. The cauliflower structure is composed of the lump-type oxides (about 12 μm) that contain the numerous granular oxides with about 0.15 μm diameter.

The oxides growing in the NaOH solution also show the slight difference on the growth rate of the oxide layer depending on the crystal orientation of zirconium metal grains. These morphologies are related to the low concentration of oxygen vacancy due to the hard Na^+-incorporation into the zirconium oxide. In the NaOH solution, the Na^+-incorporation into the zirconium oxide does not significantly contribute to the overall corrosion reaction. Therefore, the corrosion rate in the NaOH solution is lower than that in the LiOH solution and the gap in the growth rate of oxide between metal grains is gradually reduced with increasing the weight gain. At last, the oxides formed in a NaOH solution for long-term tests (200 days) are transformed into the mixed morphologies of the lump-type oxides ($d2$, about 6 μm) and the ice-columnar oxides ($d2'$, about 2.5 μm).

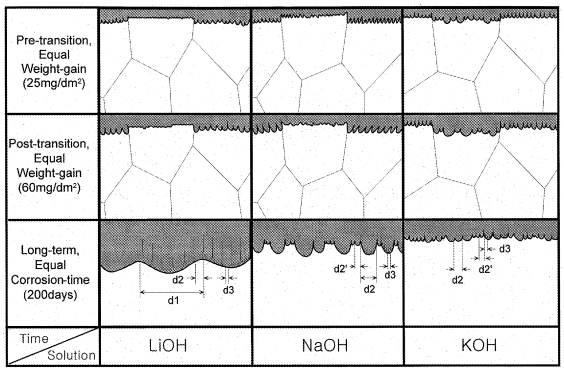

Fig. 12. Development of oxide morphology with increasing the weight gain in LiOH, NaOH and KOH solution.

In the KOH solution, the oxides having the diameter of $d2$ (about 3 μm) are observed even in the earlier stage without the large difference of the oxide growth rate between metal grains. The oxides growing in a KOH solution can keep the uniform interface at the metal–oxide interface where the local concentration of stress in the oxide does not occur.

It is observed from the TEM studies that even if the oxides have an equal thickness, the different microstructures are formed in each alkali hydroxide solutions. In the LiOH solution, the equiaxed grain is formed in both transition regimes, in the NaOH solution, the columnar grain is formed in pre-transition regime and the equiaxed grain in post-transition regime and in the KOH solution the columnar grain is formed in both transition regimes.

On the basis of the corrosion evaluation in various alkali hydroxide solutions for 300 days and the microstructural studies on the oxide using TEM and SEM, it can be suggested that the defects of oxide due to substitution of Li^+ for Zr^{4+} in the barrier layer play an important role to control the corrosion rate in early stage in low concentration of Li^+. However, Li^+ ion has also strong effect on the transformation of oxide morphology in high concentration of Li^+ ion. If the fine equiaxed oxide is formed in barrier layer, the corrosion process would be controlled by the oxide morphology.

5. Conclusions

Among the various alkali hydroxides with equimolar M^+ and OH^-, only the LiOH significantly accelerates and NaOH slightly accelerates the corrosion rate of Zircaloy-4. But in other alkali hydroxides such as KOH, RbOH and CsOH, the corrosion acceleration is not observed. The hydrogen pickup fraction also shows the similar trend to the corrosion behavior in alkali hydroxides. The cation in alkali hydroxide solutions is thought of as a responsible species on the accleration of corrosion where the ionic radius of cation would control the corrosion.

It is observed from the TEM studies on the oxides that even if the oxides have an equal thickness, the different oxide microstructures are formed depending on the alkali hydroxides. In the LiOH solution, the equiaxed grain is formed in post-transition regime as well as in pre-transition regime, in the NaOH solution the columnar grain is formed in pre-transition regime and the equiaxed grain in post-transition regime and in the KOH solution the columnar grain is formed in both transition regimes.

The different corrosion rates in equimolar alkali hydroxide solutions and the different microstructures on the oxides having an equal thickness would be caused by the probability of the cation incorporation into

zirconium oxide, on the basis of the ionic radius of cation. It can be proposed that the cation ion in the alkali hydroxide solutions would control the oxide microstructure, the oxide growth mechanism and corrosion rate in alkali hydroxide solutions.

References

[1] F. Garzarolli, J. Pohlmeyer, S. Trapp-Pritsching, H.G. Weldinger, in: Proceedings of Technical Committee Meeting on Fundamental Aspects of Corrosion on Zirconium Base Alloys, Portland, Oregon, USA, 1989, p. 34.
[2] S.G. McDonald, G.P. Sabal, K.D. Sheppard, Zirconium in the Nuclear Industry, ASTM STP 824 (1984) 519.
[3] E. Hillner, J.N. Chirigos, The effect of lithium hydroxide and related solutions on the corrosion rate, Bettis Atomic Power Laboratory Report WAPD-TM-307, 1962.
[4] R.A. Perkins, R.A. Busch, Zirconium in the Nuclear Industry, ASTM STP 1132 (1991) 595.
[5] I.L. Bramwell, P.D. Parsons, D.R. Tice, Zirconium in the Nuclear Industry, ASTM STP 1132 (1991) 628.
[6] N. Ramasubramanian, P.V. Balakrishnan, Zirconium in the Nuclear Industry, ASTM STP 1245 (1994) 378.
[7] N. Ramasubramanian, N. Precoanin, V.C. Ling, Zirconium in the Nuclear Industry, ASTM STP 1023 (1989) 187.
[8] N. Ramasubramanian, Zirconium in the Nuclear Industry, ASTM STP 1132 (1991) 613.
[9] B. Cox, C. Wu, J. Nucl. Mater. 199 (1993) 272.
[10] B. Cox, M. Ungurelu, Y.M. Wong, C. Wu, Zirconium in the Nuclear Industry, ASTM STP 1295 (1996) 114.
[11] Y.H. Jeong, H. Ruhmann, F. Garzarolli, IAEA-TECDOC-972, in: Proceedings of a IAEA Technical Committee Meeting on Influence of Water Chemistry on Fuel Cladding Behavior, Rez, Czech Republic, 1993, p. 161.
[12] F. Garzarolli, H. Seidel, R. Tricot, J.P. Gros, Zirconium in the Nuclear Industry, ASTM STP 1132 (1991) 395.
[13] H.J. Beie, A. Mitwalsky, F. Garzarolli, H. Ruhmann, H.J. Sell, Zirconium in the Nuclear Industry, ASTM STP 1245 (1994) 615.
[14] D. Pêcheur, J. Godlewski, P. Billot, J. Thomazet, Zirconium in the Nuclear Industry, ASTM STP 1295 (1996) 94.
[15] H. Anada, K. Takeda, Zirconium in the Nuclear Industry, ASTM STP 1295 (1996) 35.
[16] B. Cox, Prog. Nucl. Energy 4 (1961) 166.
[17] T. Ahmed, L.H. Keys, J. Less-common Met. 39 (1975) 99.
[18] J. Godlewski, J.P. Gros, M. Lambertin, J.F. Wadier, H. Weidinger, Zirconium in the Nuclear Industry, ASTM STP 1132 (1991) 416.
[19] H.R. Peters, Zirconium in the Nuclear Industry, ASTM STP 824 (1984) 507.
[20] J.D. McCullough, K.N. Trueblood, Acta Crystallogr. 12 (1959) 507.
[21] P. Pemsler, J. Electrochem. Soc. 105 (1958) 315.
[22] A.E. Bibb, J.R. Fascia, Trans. Metal Soc. AIME 230 (1964) 415.
[23] B. Cox, J.P. Pemsler, J. Nucl. Mater. 28 (1968) 73.